A Systematic K-edge X-ray Absorption Spectroscopic Study of Cu(III) Sites

Jennifer L. DuBois,[†] Pulakesh Mukherjee,[†] T. D. P. Stack,*[,†] Britt Hedman,*[,†,‡] Edward I. Solomon,*[,†] and Keith O. Hodgson*[,†,‡]

Contribution from the Department of Chemistry, Stanford University, Stanford, California 94305, and the Stanford Synchrotron Radiation Laboratory, SLAC, Stanford, California 94309

Received August 30, 1999

Abstract: Highly oxidized metals are constituents of oxidants, reactive intermediates, and materials with interesting conductive and magnetic properties. High-energy spectroscopies have played an important role in identifying and describing the bonding character of highly oxidized metals in these materials. A systematic study of Cu(III) K-edge X-ray absorption spectra was carried out to identify analytically useful signatures of Cu(III) in the K-edge, and to elucidate bonding descriptions for Cu(III)-containing complexes. K-edges for six Cu(III) complexes and their same-ligand Cu(II) counterparts are compared. Edges for the Cu(III) species generally appear at higher energies than their Cu(II) counterparts, though energy shifts between most individual edge features vary. However, for all Cu(III) compounds studied, the 1s → 3d transition in the preedge energy range exhibits a distinct, 2 eV shift to higher energy, relative to the known and relatively unvarying energy of the 1s → 3d transition in Cu(II) species. This energy shift provides a direct means of distinguishing Cu(III) from Cu(II). The K-edge for a complex containing Cu(II) coordinated to a 1e$^-$-oxidized ligand (phenoxyl) does not show such a change in the 1s → 3d transition energy. The analytical potential of the Cu K-edge was tested with good success using a mixed-valent trinuclear species. Cu(III) is detectable using the K-edge. The limitations of the K-edge as a Cu(III) analytical probe are discussed. An analysis applied to the 1s → 4p and 1s → 4p + shakedown transitions in the edge for a $\{Cu^{II}_2(\mu\text{-}OH)_2\}^{2+}$ dimer, using a configurational interaction (CI) model, predicted ∼75% d-character in the ground state. A similar analysis of the K-edge for $\{Cu^{III}_2(\mu\text{-}O)_2\}^{2+}$ indicates that the Cu in this complex has far more covalent bonds with the oxo bridging ligands (d-character ∼60%).

Introduction

Copper in its unusual trivalent oxidation state has been a subject of chemical and theoretical interest over the past two decades. Cu(III) has been proposed as a constituent of synthetic oxidants,[1,2] as a reactive intermediate in oxidative processes,[3] and as a key component of the cuprate family of superconductors.[1] In addition, the chemistry of Cu(III) in a polypeptide environment has been studied in great detail.[2−4] Yet, spectroscopic means of identifying or describing the bonding character of Cu(III) in many of these materials are not well developed.

Metalloenzymes that catalyze 2-electron (2e$^-$) oxidations at single-copper active sites are known (e.g., galactose oxidase (GO),[5] dopamine β-monooxygenase (DβM),[6] and peptidyl-hydroxylating monooxygenase (PHM)[7]). The reactive species in GO contains a Cu(II) ion coordinated to the 1e$^-$-oxidized phenolate group of a tyrosine residue, and not Cu(III).[8−10] The electronic character of the reactive species in DβM and PHM is still the subject of current research. Well-characterized synthetic species containing similar $\{Cu^{II}\text{-}\underline{O}\text{-}R\}$ (R = substituted phenyl ring; $\underline{O}$ = an oxygen-centered electron hole) units are known,[11−16] as are molecules containing the formally isoelectronic $\{Cu^{III}\text{-}O^{2-}\text{-}X\}$ (X = Cu^{III}) unit.[17−19] Differences in

* To whom correspondence should be addressed.
[†] Department of Chemistry, Stanford University.
[‡] Stanford Synchrotron Radiation Laboratory.

(1) For example: (a) Whangbo, M. H.; Kang, D. B.; Torardi, C. C. *Physica C* **1989**, *158*, 371−376. (b) Whangbo, M.-H.; Torardi, C. C. *Science* **1990**, *249*, 1143−1146. (c) Tarascon, J. M.; Greene, L. H.; Barboux, P.; McKinnon, W. R.; Hull, G. W.; Orlando, T. P.; Delin, K. A.; Foner, S.; McNiff, E. J. *Phys. Rev. B* **1987**, *36*, 8393−8400.

(2) Margerum, D. W.; Scheper, W. M.; McDonald, M. R.; Fredericks, F. C.; Wang, L.; Lee, H. D. *Bioinorganic Chemistry of Copper*; Karlin, K. D., Tyeklár, Z., Eds.; Chapman & Hall: New York, 1993; pp 213−221.

(3) McDonald, M. R.; Fredericks, F. C.; Margerum, D. W. *Inorg. Chem.* **1997**, *36*, 3119−3124.

(4) Lockwood, M. A.; Blubaugh, T. J.; Collier, A. M.; Lovell, S.; Mayer, J. M. *Angew. Chem., Int. Ed. Engl.* **1999**, *38*, 225−227.

(5) Whittaker, M. M.; Whittaker, J. W. *J. Biol. Chem.* **1990**, *265*, 9610−9613.

(6) Klinman, J. P. *Chem. Rev.* **1996**, *96*, 2541−2561.

(7) Prigge, S. T.; Kolhekar, A. S.; Eipper, B. A.; Mains, R. E.; Amzel, L. M. *Science* **1997**, *278*, 1300−1305.

(8) Clark, K.; Penner-Hahn, J. E.; Whittaker, M. M.; Whittaker, J. W. *J. Am. Chem. Soc.* **1990**, *112*, 6433−6434.

(9) Clark, K.; Penner-Hahn, J. E.; Whittaker, M. M.; Whittaker, J. W. *Inorg. Chem.* **1994**, *33*, 12553−12557.

(10) Knowles, P. F.; Brown, R. D., III; Koenig, S. H.; Wang, S.; Scott, R. A.; McGuirl, M. A.; Brown, D. E.; Dooley, D. M. *Inorg. Chem.* **1995**, *34*, 3895−3902.

(11) Wang, Y.; Stack, T. D. P. *J. Am. Chem. Soc.* **1996**, *118*, 13097−13098.

(12) Wang, Y.; DuBois, J. L.; Hedman, B.; Hodgson, K. O.; Stack, T. D. P. *Science* **1998**, *279*, 537−540.

(13) Müller, J.; Weyhermüller, T.; Bill, E.; Hildebrandt, P.; Ouldmoussa, L.; Glaser, T.; Wieghardt, K. *Angew. Chem., Int. Ed. Engl.* **1998**, *37*, 616−619.

(14) Chaudhuri, P.; Hess, M.; Flörke, U.; Wieghardt, K. *Angew. Chem., Int. Ed. Engl.* **1998**, *37*, 2217−2220.

(15) Whittaker, M. M.; Kersten, P. J.; Nakamura, N.; Sanders-Loehr, J.; Schweizer, J. W.; Whittaker, J. W. *J. Biol. Chem.* **1996**, *271*, 681−687.

(16) Halfen, J. A.; Young, V. G., Jr.; Tolman, W. B. *Angew. Chem., Int. Ed. Engl.* **1996**, *35*, 1687−1690.

(17) Tolman, W. B. *Acc. Chem. Res.* **1997**, *30*, 227−237.

10.1021/ja993134p CCC: $19.00
Published on Web 06/06/2000

copper−oxygen bonding character in such formally isoelectronic Cu/O species, which may translate into different modes of reactivity, remain to be fully described.

High-energy (i.e., soft/hard X-ray) spectroscopies are particularly well suited to directly probing Cu(III), as well as differences with isoelectronic {Cu^{II}-$\underline{L}$} species ($\underline{L}$ = ligand-centered electron hole), due to their ability to access core electrons. Core electrons on Cu(III) should have an increased binding energy relative to core electrons on Cu(II), due to the greater effective nuclear charge on the more highly oxidized copper. Effects of increased effective nuclear charge should be felt most strongly by the least shielded core electrons; these in turn are least perturbed by chemical changes, which significantly impact valence (d orbital) electrons. It is especially useful to define core−electronic shifts as Cu(III) and {Cu^{II}-$\underline{L}$} are frequently diamagnetic species,[20] and thus are inaccessible by magnetic techniques. Similarly, Cu(II) ions bridged by oxygen ligands are often diamagnetic, due to strong antiferromagnetic coupling between the unpaired copper electrons.

A number of hard and soft X-ray studies have been performed on solid-state materials, particularly within the family of cuprate superconductors, with the aim of determining Cu(III) content in mixed-valence materials.[21−26] Many of these studies suffer from the complexity of the materials under study, from effects on the spectra due to long-range order in the solid-state material, or from a lack of basic information on the Cu(III) K-edge, due to the relatively small number of reference spectra collected on well-characterized Cu(III) species.

Recently, Cu K-edge X-ray absorption spectroscopy[27] (XAS) was used to assign the oxidation state of the copper in thermally sensitive molecules containing a $\{Cu_2(\mu\text{-}O)_2\}^{2+}$ unit.[28] Comparison of edges for these molecules to edges for the analogous $\{Cu^{II}_2(\mu\text{-}OH)_2\}^{2+}$ molecules with the same ligands, as well as to Cu K-edges for several reference compounds, led to the description of the coppers as Cu(III). Cu K-edge XAS was especially appropriate as compared to photoelectron spectroscopy because it is a bulk-sample, high-energy technique that does not require ultrahigh vacuum. Thermally sensitive materials are therefore easily accommodated, and surface impurities on samples do not significantly complicate the data. For similar reasons, this technique is also well-suited for trapped reactive intermediates and for samples in dilute solution.

Scheme 1. Diagrams of Selected Complexes Used in This Study[a]

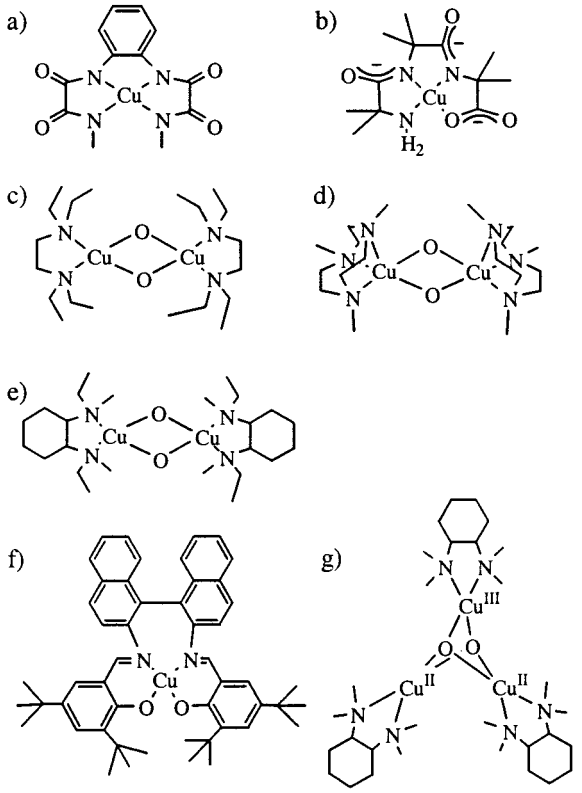

[a] (a) $[Cu^{III}(H_{-3}Aib_3)]$; (b) $[Cu^{III}L^3][PPh_4]$; (c) $[Cu^{III}_2(\mu\text{-}O)_2(L_{TEED})_2]^{2+}$; (d) $[Cu^{III}_2(\mu\text{-}O)_2(L_{Me_3TACN})_2]^{2+}$; (e) $[Cu^{III}_2(\mu\text{-}O)_2(L_{ME})_2]^{2+}$; (f) $[Cu^{II}BDB]$; (g) $[Cu^{II}Cu^{II}Cu^{III}O_2(L_{TM})_3]^{3+}$.

In this paper the K-edge data set is expanded to include several pairs of simple, analogous Cu(II)/Cu(III)-containing molecules, spanning a variety of geometries and coordination environments (Scheme 1). A primary objective is to determine if Cu(III)-specific edge features exist. Such features provide a basis for using Cu K-edge XAS as an analytical method to identify Cu(III). A second objective is to present a self-consistent and quantitative description of the Cu(III) K-edge spectrum. Such a description adds to the current understanding of Cu(III)-ligand bonding (notably, the $Cu^{III}-O^{2-}$ bond), and expands previous systematic studies of Cu(II) and Cu(I) edges[29] to the Cu(III) K-edge. Further, the Cu(III) K-edge can be contrasted to data for the isoelectronic {Cu^{II}-$\underline{O}$-R} structure, to begin to describe differences in bonding between these complexes. Finally, K-edge data for a related $Cu^{II}Cu^{II}Cu^{III}$ localized mixed-valence cluster[30] are presented. These data directly test the applicability of Cu K-edge spectroscopy to deconvolute Cu(III)/Cu(II) mixtures.

Experimental Section

Sample Preparation and Data Collection. Compounds were prepared according to published procedures.[18,31−34] CuO, $(creatininium)_2[CuCl_4]$, $Cs_2[CuCl_4]$, $[CuImH_4](NO_3)_2$ (ImH = imidazole), and [Cu-

(18) Mahadevan, V.; Hou, Z. G.; Cole, A. P.; Root, D. E.; Lal, T. K.; Solomon, E. I.; Stack, T. D. P. *J. Am. Chem. Soc.* **1997**, *119*, 11996−11997.

(19) Karlin, K. D.; Kaderli, S.; Zuberbühler, A. D. *Acc. Chem. Res.* **1997**, *30*, 139−147.

(20) The unpaired electron on the Cu(II) antiferromagnetically couples to the unpaired electron on the coordinated phenoxyl, producing an $S = 0$ ground state. Cu(II)-phenoxyl species with $S = 1$ ground states are also known (ref 9). At least two paramagnetic ($S = 1$ ground state) Cu(III) species are known: an octahedral CuS_6 complex (Krebs, C.; Glaser, T.; Bill, E.; Weyhermüller, T.; Meyer-Klaucke, W.; Wieghardt, K. *Angew. Chem., Intl. Ed. Engl.* **1999**, *38*, 359−361) and K_3CuF_6 (Cotton, F. A.; Wilkinson, G. *Advanced Inorganic Chemistry*, 5th ed.; John Wiley and Sons: New York, 1988; p 774).

(21) Alp, E. E.; Shenoy, G. K.; Hinks, D. G.; Capone, D. W., II.; Soderholm, L.; Schuttler, H. B.; Guo, J.; Ellis, D. E.; Montano, P. A.; Ramanathan, M. *Phys. Rev. B* **1987**, *35*, 7199−7202.

(22) Boyce, J. B.; Bridges, F.; Claeson, T.; Howland, R. S.; Geballe, T. H. *Phys. Rev. B* **1987**, *36*, 5251−5257.

(23) Choy, J. H.; Kim, D. K.; Hwang, S. H.; Park, J. C. *J. Am. Chem. Soc.* **1995**, *117*, 7556−7557.

(24) Tranquada, J. M.; Heald, S. M.; Moodenbaugh, A. R. *Phys. Rev. B* **1987**, *36*, 5263−5274.

(25) Tranquada, J. M.; Heald, S. M.; Kunnmann, W.; Moodenbaugh, A. R.; Qiu, S. L.; Xu, Y.; Davies, P. K. *Phys. Rev. B* **1991**, *44*, 5176−5189.

(26) Stoll, S. I.; Bornick, R. M.; Stacey, A. M. *Inorg. Chem.* **1997**, *36*, 1838−1841.

(27) K-edge: the electronic absorption spectrum of the 1s electron, extending to and beyond the 1s electron binding energy.

(28) DuBois, J. L.; Mukherjee, P.; Collier, A. M.; Mayer, J. M.; Solomon, E. I.; Hedman, B.; Stack, T. D. P.; Hodgson, K. O. *J. Am. Chem. Soc.* **1997**, *119*, 8578−8579.

(29) Kau, L.-S.; Spira-Solomon, D. J.; Penner-Hahn, J. E.; Hodgson, K. O.; Solomon, E. I. *J. Am. Chem. Soc.* **1987**, *109*, 6433−6442.

(30) Cole, A. P.; Root, D. E.; Mukherjee, P.; Solomon, E. I.; Stack, T. D. P. *Science* **1996**, *273*, 1848−1850.

(31) Mahapatra, S.; Halfen, J. A.; Wilkinson, E. C.; Pan, G. F.; Wang, X. D.; Young, V. G.; Cramer, C. J.; Que, L., Jr.; Tolman, W. B. *J. Am. Chem. Soc.* **1996**, *118*, 11555−11574.

Table 1. Cu(II)/Cu(III) Compounds Used, Their Geometries, and Results to Fits to Preedge (1s → 3d) Transitions

compd	ligation	preedge energy[a]	preedge intensity[a,b]	ref
$[Cu^{III}(H_{-3}Aib_3)]$	N_3O	8980.99(0.02)	1.4(0.04)	33
$[Cu^{II}H_{-2}Aib_3)]_2$		8978.78(0.02)	1.7(0.18)	33, 2
$[Cu^{III}L^3][PPh_4]$	N_4	8980.84(0.06)	1.0(0.08)	32
$[Cu^{II}L^3][PPh_4]_2$		8978.75(0.06)	1.2(0.14)	32
$KCu^{III}O_2$	O_4	8981.04(0.08)	1.5(0.07)	34a
$Cu^{II}O$		8979.14(0.10)	0.97(0.03)	34b
$[Cu^{III}_2(\mu\text{-}O)_2(L_{ME})_2]^{2+}$	N_2O_2	8980.93(0.06)	1.5(0.03)	18
$[Cu^{II}_2(\mu\text{-}OH)_2(L_{ME})_2]^{2+}$		8979.08(0.02)	1.2(0.11)	18
$[Cu^{III}_2(\mu\text{-}O)_2(L_{Me_3-TACN})_2]^{2+}$	N_3O_2	8980.48(0.07)	1.7(0.11)	31
$[Cu^{II}_2(\mu\text{-}OH)_2(L_{Me3-TACN})_2]^{2+}$		8978.67(0.07)	2.2(0.09)	31
$[Cu^{III}_2(\mu\text{-}O)_2(L_{TEED})_2]^{2+}$	N_2O_2	8980.84(0.06)	1.2(0.16)	18
$[Cu^{II}_2(\mu\text{-}OH)_2(L_{TEED})_2]^{2+}$		8978.82(0.10)	1.3(0.13)	18
Cu^{II}BDB	N_2O_2	8979.18(0.01)	1.5(0.10)	11
Cu^{II}-O-BDB		8979.14(0.01)	0.97(0.08)	11

[a] Preedge energies and intensities are derived from fits to the data (see Experimental Section for details). Numbers in parentheses are standard deviations for the measured quantities, over three fitting ranges. [b] Values reported for preedge peak intensities were multiplied by 100.

$(acac)_2$] (acac = acetylacetonate) were purchased. Dry solid samples were diluted in boron nitride and the mixtures ground into fine powder. Air and thermally sensitive materials were handled at low temperature (−78 °C) and/or under inert N_2 atmosphere throughout to prevent sample degradation. The mixtures were pressed into 1 mm thick aluminum spacers lined with Mylar tape (X-ray transparent) windows. X-ray absorption spectra were measured on unfocused wiggler beamline 7-3 at the Stanford Synchrotron Radiation Laboratory (SSRL), with the ring operating at 3 GeV and 50−100 mA. Samples were maintained at 10 K inside an Oxford Instruments CF-1208 liquid helium continuous flow cryostat. A Si(220) double-crystal monochromator was used, detuned 50% at 9868 eV to minimize contamination of the radiation by higher harmonics. Vertical 1 mm pre-monochromator slits were used to define the beam size, minimizing beam divergence. K-edge and EXAFS data were measured, for all samples, over the energy range 8650−9868 eV. The monochromator step size in the edge region (8970−9020 eV) was 0.1−0.2 eV, to enhance resolution over this range. Spectra were collected in transmission mode, using N_2 filled ionization chambers to measure the intensity of incident and transmitted radiation. The spectrum of a Cu foil was collected concomitantly, allowing for internal energy calibration of the spectra. The first inflection point energy for the Cu foil spectra was set to 8980.3 eV. The spectrometer energy resolution was approximately 1.4 eV,[35] with reproducibility in the determination of edge position of <0.2 eV. Two to four scans were averaged for each data set. Though EXAFS data were collected to $k = 15$ Å^{-1}, some spectra were truncated at 13 Å^{-1} due to interference from small amounts of zinc contamination in the samples.

Data Reduction and Analysis. For each spectrum, a smooth second-order polynomial was fit to the preedge region, then extrapolated and subtracted from the data. A spline was fit and subtracted from the EXAFS region, and the data normalized at 9000 eV, using the *SPLINE* program (written by Dr. Paul Ellis, SSRL). The three-region spline was of orders 2, 3, 3, defined by the energy points (eV) 9010, 9100, 9300, 9868 (or 9640 for spectra truncated at $k = 13$ Å^{-1}). EXAFS data for each compound were analyzed (data and analysis not shown) as a check on the structural integrity, and hence the purity, of each of the samples. Theoretical phase and amplitude functions derived from *feff* 6.0[36] were used in creating a calculated EXAFS spectrum, which was adjusted by a least-squares fitting process to match the data (using the EXAFSPAK programs which utilize the public domain MINPAK fitting library[37]).[38] Absorber−scatterer distances and Debye−Waller factors (σ^2) were varied for each equivalent set of backscattering atoms, and coordination numbers were kept constant. In all possible cases, the agreement between structural conclusions from EXAFS data and crystal structures was excellent.

The intensities and energies of the preedge features for each edge were quantified by least-squares fits of pseudo-Voigt line shapes to the data (half-Gaussian, half-Lorentzian peaks).[39] Fits were performed using the EDG_FIT program.[38] The energy position, full-width at half-maximum (fwhm), and peak height for each preedge were varied. The background rising-edge absorption over the entire fitting range (three ranges used: 8976−8983, 8976−8984, and 8976−8985 eV) was modeled by an additional pseudo-Voigt line or lines. Fits were done concurrently to data and second derivatives of the data, taking advantage of the ability of the second derivative to highlight positions of peaks obscured behind background absorption. The approximate peak intensity for preedges is given as height × fwhm. As widening the energy range over which fits were carried out gave slightly variable results to the fits (due to the inability to precisely model background absorption from the rising edge), the previously mentioned three energy ranges were used. Results from the three fits were averaged. Average results are given in Table 1. To estimate the variability of fits, standard deviations for peak heights and intensities, from fits over each of the energy ranges used, were calculated.

For further analysis of the structure of edges measured for $[Cu^{III}_2(\mu\text{-}O)_2(L_{ME})_2]^{2+}$ and $[Cu^{II}_2(\mu\text{-}OH)_2(L_{ME})_2]^{2+}$ (L_{ME} defined below), an approximate fit of three peaks (two-half-Gaussian/half-Lorentzian, one Gaussian) plus a 50%−erf/50%−arctangent curve to simulate the edge jump was carried out over the energy range 8976−9005 eV (where erf is the error function, $\mathrm{erf}(x) = 2/\sqrt{\pi}\int_0^x e^{-t^2}dt$). Second derivative spectra as well as raw data were used as guides in determining the number and energy positions of peaks. This fitting rationale was chosen to be consistent with previous fits to *z*-polarized K-edge data.[40] In prior work, three peaks were needed to fit the spectra adequately,[39] corresponding to two intense, narrow absorption lines (the two pseudo-Voigt, half-Gaussian/half-Lorentzian peaks) with a much broader absorption between them (fit with a Gaussian line shape). The narrow lines were assigned as 1s → 4p and 1s → 4p + shakedown peaks (vide infra); the broader peak was not assigned. It likely has contributions from *xy*-polarized absorption in the case of nonpolarized data, and may also include background absorption not sufficiently accounted for by the 50%−erf/50%−arctangent curve. Absorption in this range may also reflect additional, higher-energy shakedown events. The broader peak

(32) Ruiz, R.; Surville-Barland, C.; Aukauloo, A.; Anxolabéhère-Mallart, E.; Journaux, Y.; Cano, J.; Muñoz, M. C. *J. Chem. Soc., Dalton Trans.* **1997**, 745−751.

(33) Diaddario, L. L.; Robinson, W. R.; Margerum, D. W. *J. Am. Chem. Soc.* **1983**, *22*, 1021−1025.

(34) (a) Costa, G. A.; Kaiser, E. *Thermochim. Acta* **1995**, *269/270*, 591−598. (b) Åsbrink, S.; Waskowska, A. *J. Phys. Cond. Matter* **1991**, *3*, 8173−8180.

(35) Lytle, F. W. *Applications of Synchrotron Radiation*; Winick, H., Xiam, D., Ye, M.-H., Huang, T., Eds.; Gordon and Breach Science Publishers: New York, 1989; pp 135−223.

(36) Mustre de Leon, J.; Rehr, J. J.; Zabinsky, S. I.; Albers, R. C. *Phys. Rev. B* **1991**, *44*, 4146−4156.

(37) Garbow, B. S.; Hillstrom, K. E.; More, J. J., Argonne National Laboratory.

(38) The EXAFSPAK programs (including EDG_FIT) were written by Dr. Graham N. George, SSRL. They may be obtained free at the following web site: http://www-ssrl.slac.stanford.edu/exafspak.html.

(39) Shadle, S. E.; Penner-Hahn, J. E.; Schugar, H. J.; Hedman, B.; Hodgson, K. O.; Solomon, E. I. *J. Am. Chem. Soc.* **1993**, *115*, 768−776.

(40) Smith, T. A.; Penner-Hahn, J. E.; Berding, M. A.; Doniach, S.; Hodgson, K. O. *J. Am. Chem. Soc.* **1985**, *107*, 5945−5955.

Table 2. Curve-Fitting Results for Edge Spectra for $[Cu^{II}_2(\mu\text{-}OH)_2(L_{ME})_2]^{2+}$ and $[Cu^{III}_2(\mu\text{-}O)_2(L_{ME})_2]^{2+}$

	fit		peak 1[a] (shakedown)	peak 2	peak 3 (main peak)	arctan/erf	R^b
$[Cu^{II}_2(\mu\text{-}OH)_2(L_{ME})_2]^{2+}$	1	energy[c]	8985.95	8990.46	8993.30	8994.50	5.61×10^{-4}
		height	0.298	0.487	0.525	1.12	
		fwhm	1.68	2.90	1.50	1.38	
	2	energy	8985.96	8990.45	8993.32	8994.50	5.24×10^{-4}
		height	0.300	0.487	0.558	1.12	
		fwhm	1.70	2.90	1.40	1.45	
	3	energy	8985.90	8990.32	8993.33	8994.51	5.48×10^{-4}
		height	0.297	0.482	0.553	1.12	
		fwhm	1.65	2.96	1.45	1.35	
	4	energy	8985.96	8990.40	8993.30	8994.52	5.72×10^{-4}
		height	0.287	0.463	0.569	1.12	
		fwhm	1.75	3.00	1.42	1.35	
	av	energy	8985.96 (0.03)[d]		8993.31 (0.02)		
		height	0.295 (0.006)		0.551 (0.019)		
		fwhm	1.69 (0.04)		1.44 (0.04)		
$[Cu^{III}_2(\mu\text{-}O)_2(L_{ME})_2]^{2+}$	1	energy	8987.10	8993.27	8995.80	8997.15	1.50×10^{-4}
		height	0.470	0.547	0.300	1.10	
		fwhm	1.45	3.76	1.52	1.97	
	2	energy	8987.08	8993.28	8995.78	8997.08	1.70×10^{-4}
		height	0.440	0.557	0.288	1.09	
		fwhm	1.49	3.81	1.38	1.98	
	3	energy	8987.05	8993.21	8995.80	8996.96	1.49×10^{-4}
		height	0.447	0.556	0.290	1.10	
		fwhm	1.53	3.68	1.38	1.93	
	4	energy	8987.10	8993.19	8995.90	8997.07	1.56×10^{-4}
		height	0.450	0.541	0.311	1.10	
		fwhm	1.50	3.71	1.50	1.99	
	av	energy	8987.08 (0.02)		8995.82 (0.05)		
		height	0.452 (0.013)		0.297 (0.010)		
		fwhm	1.49 (0.03)		1.44 (0.07)		

[a] See text for complete description of lineshapes used and peak assignments. [b] R = least-square residual function. [c] Energies given in eV. [d] Numbers in parentheses are standard deviations.

compensates for all of these contributions to the absorption spectrum in an approximate way.

Peak intensities measured here are to be considered somewhat approximate, since the 1s → 4p and 1s → 4p + shakedown transitions are *z*-polarized[40] and the data used were unpolarized. Even when *z*-polarized data are used, it has been shown that peak intensities are still difficult to measure precisely, because of the inability to reliably simulate the background of the rising edge absorption.[39] Peak energies were easier to determine, as minima in second derivative spectra were clearly visible. The three peaks were first fit to the data, allowing their energies, heights, and fwhm to vary. The arctangent/erf curve was then added to the fit. Its inflection point energy and its width were varied, along with the energies, heights, and fwhms of the three peaks, to produce the best fit to the data. Because the background absorption could not be precisely modeled, a number of fits to the data were performed with varying background features. Results from four such statistically comparable fits (i.e., fits having similar least-squares residuals) were averaged. Peak energies and their estimated intensities are given in Table 2, with standard deviations for each averaged quantity.

Results and Analysis

Cu(II)/Cu(III) Edge Pairs. Cu K-edge XAS spectra were measured for six different chemically and, in most cases, crystallographically characterized Cu(III) compounds along with their Cu^{II} counterpart species having identical or nearly identical ligands (Figure 1). These compounds were selected to span a range of geometries and O/N ligand environments, and many of the available chemical types of known Cu(III) compounds (Scheme 1). These include square-planar, solid-state O_4-ligated $KCu^{III}O_2$;[34] square-planar, N_2O_2 molecular $[Cu^{III}_2O_2(L_{ME})_2]^{2+}$ (L_{ME} = (1*R*,2*R*)-trans-*N*,*N*′-diethyl-*N*,*N*′-dimethylcyclohexanediamine);[18] square-planar, N_2O_2 $[Cu^{III}_2O_2(L_{TEED})_2]^{2+}$ (L_{TEED} = *N*,*N*,*N*′,*N*′-tetraethylethylenediamine);[18] 5-coordinate (square pyramidal) $[Cu^{III}_2O_2(L_{Me_3TACN})_2]^{2+}$ (L_{Me_3TACN} = 1,4,7-trimethyl-1,4,7-triazacyclononane);[31] a mono-copper/N_4-ligated, square-planar complex, $[Cu^{III}L^3][PPh_4]$ (L^3 = *N*,*N*′-*o*-phenylenebis(oxamate) bis(methylamide));[32] and the mono-copper, tripeptide ligated (N_3O), classic Cu(III) complex $[Cu^{III}(H_{-3}Aib)]$ (Aib = tri-α-aminoisobutyric acid).[4,33] These compounds and their respective, same-ligand Cu^{II} counterpart species are listed in Table 1. Note that this study does not include sulfur-ligated Cu(III) species, though a limited number of these are known to exist.[41,42]

Cu K-edge data for each Cu(II)/Cu(III) pair are presented in Figure 1. Because metal K-edge structure varies with the number, type, and geometric arrangement of the ligands, as well as the oxidation state of the metal, varying only one of these parameters at a time allows for the best comparisons between edges.[29,43−45] Hence, the best measure of oxidation-state-dependent changes in metal K-edges comes from comparing pairs of otherwise equivalent complexes (Figure 2). The most obvious effect of changing oxidation state evident in these edge pairs is an overall shift in the entire Cu(III) edge spectrum to higher energy, relative to the Cu(II) edge. Individual features on each edge are also energy-shifted to different degrees in the Cu(III) edges.

Edge Features and Their Assignments. Structure-contributing peaks on and above the broad absorption of the rising edge

(41) Hanss, J.; Kruger, H. J. *Angew. Chem., Int. Ed. Engl.* **1997**, *35*, 2827−2830.
(42) Krebs, C.; Glaser, T.; Bill, E.; Weyhermüller, T.; Meyer-Klaucke, W.; Wieghardt, K. *Angew. Chem., Int. Ed. Engl* **1999**, *38*, 359−361.
(43) Colpas, G. J.; Maroney, M. J.; Bagyinka, C.; Kumar, M.; Willis, W. S.; Suib, S. L.; Baidya, N.; Mascharak, P. K. *Inorg. Chem.* **1991**, *30*, 920−928.
(44) Penner-Hahn, J. E.; Fronko, R. M.; Pecoraro, V. I.; Yocum, C. F.; Betts, S. D.; Bowlby, N. R. *J. Am. Chem. Soc.* **1990**, *112*, 2549−2557.
(45) Blackburn, N. J.; Strange, R. W.; Reedijk, J.; Volbeda, A.; Farooq, A.; Karlin, K. D.; Zubieta, J. *Inorg. Chem.* **1989**, *28*, 1349−1357.

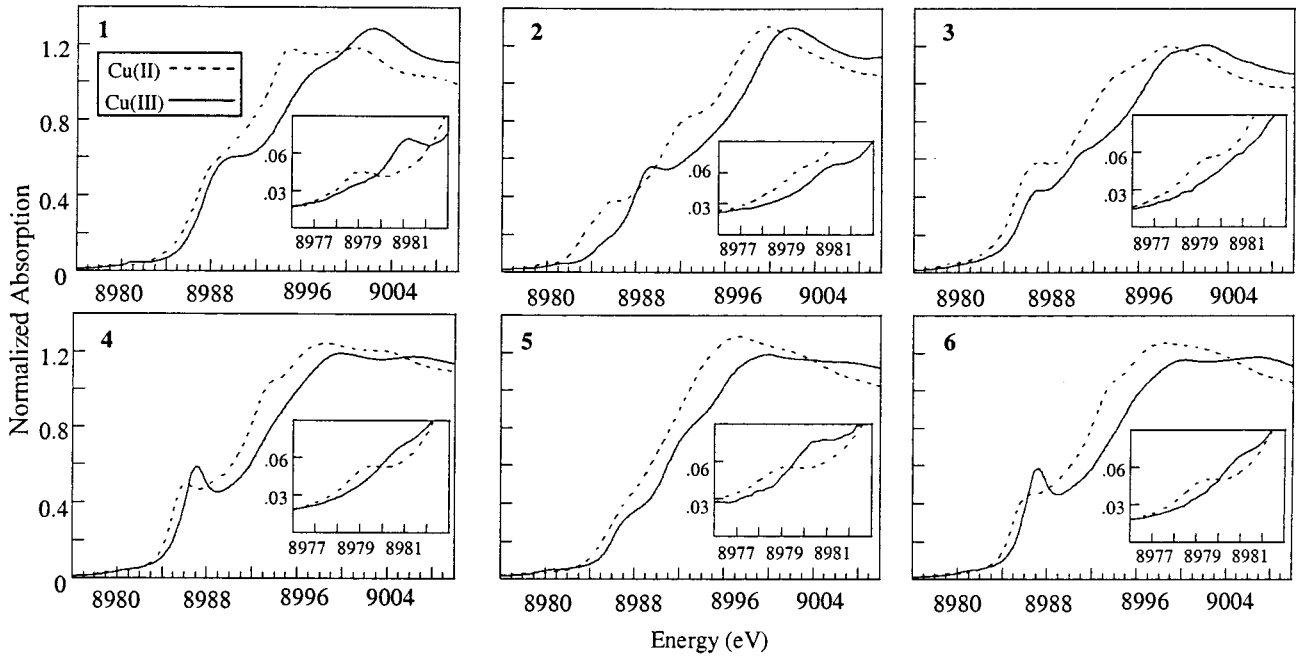

Figure 1. Cu K-edges for Cu(III) complexes (solid lines) and their analogous Cu(II) complexes (dotted lines). Insets show the amplified preedge region (i.e., location of 1s → 3d transitions) (8976−8983 eV): (1) $[Cu^{III}(H_{-3}Aib_3)]$ and $[Cu^{II}(H_{-2}Aib_3)]_2$; (2) $[Cu^{III}L^3][PPh_4]$ and $[Cu^{II}L^3][PPh_4]_2$; (3) $KCu^{III}O_2$ and CuO; (4) $[Cu^{III}_2(\mu\text{-}O)_2(L_{TEED})_2]^{2+}$ and $[Cu^{II}_2(\mu\text{-}OH)_2(L_{TEED})_2]^{2+}$; (5) $[Cu^{III}_2(\mu\text{-}O)_2(L_{Me_3TACN})_2]^{2+}$ and $[Cu^{II}_2(\mu\text{-}OH)_2(L_{Me_3TACN})_2]^{2+}$; and (6) $[Cu^{III}_2(\mu\text{-}O)_2(L_{ME})_2]^{2+}$ and $[Cu^{II}_2(\mu\text{-}OH)_2(L_{ME})_2]^{2+}$.

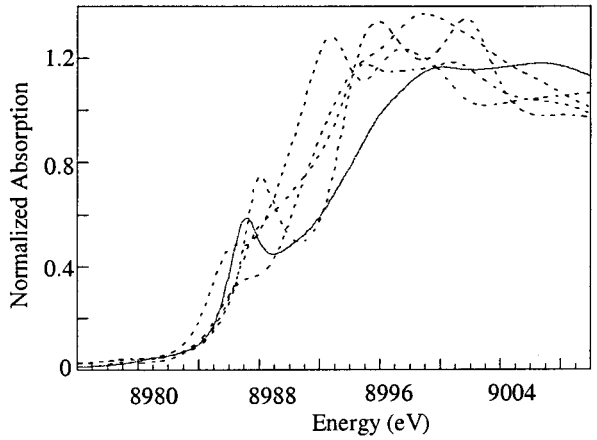

Figure 2. Cu K-edge for $[Cu^{III}_2(\mu\text{-}O)_2(L_{ME})_2]^{2+}$ (solid line) with K-edges for a variety of Cu(II) complexes (dotted lines). In order of ascending first inflection point energies, they are as follows: $CuCl_4^{2-}$ (D_{4h}), $[Cu^{II}(H_{-2}Aib)]_2$, $[Cu^{II}_2(\mu\text{-}OH)_2(L_{ME})_2]^{2+}$, $Cu^{II}(acac)_2$, $[Cu^{II}(ImH)_4]^{2+}$. Note the difficulty of assessing the oxidation state in $[Cu^{III}_2(\mu\text{-}O)_2(L_{ME})_2]^{2+}$ by comparison to edges for these non-same-ligand Cu(II) complexes.

were identified from the absorption spectrum and its second derivative. A low-intensity transition appears to the low-energy side of each edge in the preedge region, and one or two transitions appear as shoulders along the rising edge before the principal edge maximum (i.e., the point of highest absorption intensity in the edge). The edge maximum and two to three higher energy peaks are distinctly visible in all of the spectra. Cu(II) K-edges measured using polarized X-rays on oriented single crystals have determined that the preedge feature is an electric-quadrupole allowed, 1s → 3d transition.[46] The transition gains additional intensity in a noncentrosymmetric environment through 3d/4p orbital mixing, as the transition of the 1s electron to the 4p orbital is electric dipole allowed ($\Delta l = 1$) and therefore very intense. The two peaks appearing along the rising edge, between the preedge and principal maximum, have been assigned previously as a pair of 1s → 4p bound-state transitions (i.e., a larger 1s → 4p "main" peak and a secondary peak due to a 1s → 4p transition with shakedown contributions).[47,48] The origin and interpretation of these transitions will be discussed in detail in the following section. The edge absorption maximum and higher energy peaks are likely due to multiple scattering (MS) effects and thus are dependent on the local geometric rather than electronic structure of the copper.[49]

Features in the Cu(II) K-edges appear to have counterparts in the Cu(III) K-edges; in general, the Cu(III) features occur at higher energies than the equivalent features in the edge for the same-ligand Cu(II) complex. However, the absolute energies of transitions and the magnitudes of Cu(II)/Cu(III) energy shifts in most cases varied widely among the compounds studied. One notable exception is the preedge (1s → 3d) transition for all of the Cu(II) complexes measured, occurring at ∼8979 eV (± 0.3 eV) (Table 1). A prior systematic Cu K-edge study likewise showed preedge transitions within a similar energy range 8979 eV (+0.4/-0.6 eV) for 40 Cu(II) complexes with a broad variety of ligands.[29] By contrast, preedges for all of the Cu(III) complexes in this study occur at ∼8981 eV (± 0.5 eV) (Figure 1, insets; Figure 3; Table 1). No other transition appears to be this systematically shifted in edges for the Cu(III), relative to the Cu(II), complexes. For each Cu(II)/Cu(III) pair, the 1s → 4p transition occurs at higher energy for Cu(III) than for Cu(II). The magnitude of the energy shift varies between 1 and 2 eV. Shifts in the principal edge maximum (i.e., the point of highest intensity in the edge) and the following two to three peaks were on the order of 1 eV for each Cu(II)/Cu(III) edge pair.

Analysis of 1s → 4p Transitions. K-edge spectra measured for tetragonal Cu(II) complexes consistently have two *z*-

(46) Hahn, J. E.; Scott, R. A.; Hodgson, K. O.; Doniach, S.; Desjardins, S. E.; Solomon, E. I. *Chem. Phys. Lett.* **1982**, *88*, 595−598.

(47) Kosugi, N.; Yokoyama, T.; Asakuna, K.; Kuroda, H. *Chem. Phys.* **1984**, *91*, 249−256.

(48) Bair, R. A.; Goddard, W. A. *Phys. Rev. B* **1980**, *22*, 2767−2776.

(49) Lytle, F. W. *Phys. Rev. B* **1988**, *37*, 1550−1562.

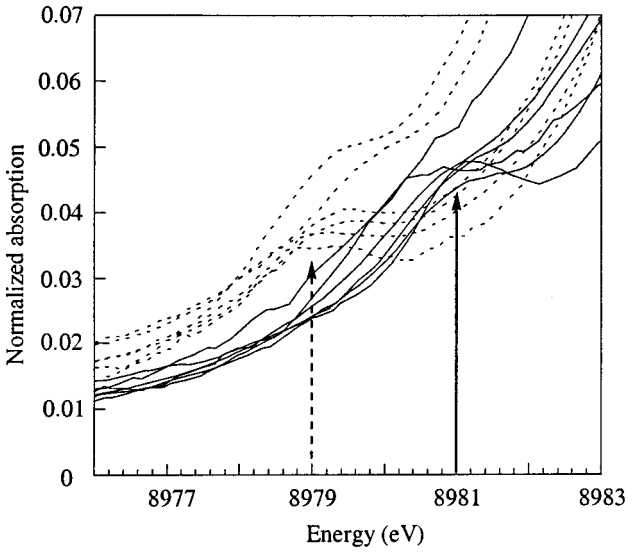

Figure 3. Comparison of preedges (1s → 3d transitions) for all 12 compounds listed in Figure 1. Data for the Cu(II) complexes are shown as dotted lines; data for Cu(III) complexes are shown as solid lines. Note the clustering of transitions around 8979 and 8981 eV for the Cu(II) and Cu(III) species, respectively.

polarized transitions[40] before the edge's principal maximum, at energies of ~8993 and 8986 eV (Figure 4).[29] These have been assigned, respectively, as a 1s → 4p transition and a 1s → 4p transition with concurrent ligand-to-metal charge transfer (LMCT), which gains intensity because of final-state relaxation (i.e., formally a 2-electron "shakedown" transition). Relaxation of the Cu electrons in the excited state occurs because of the increased effective nuclear charge felt by the electrons in the presence of a 1s core hole. Using the formalism of many-electron states, the higher energy peak can equivalently be described as a transition to the $|\underline{1s}3d^9\rangle$ final state. The lower energy peak is due to a transition to a $|\underline{1s}3d^{10}\underline{L}\rangle$ final state ($\underline{L}$ = a hole in the ligand valence p shell; $\underline{1s}$ = photoexcited 1s core hole). These assignments are consistent with calculations and have their analogues in the main and satellite peak structure observed in Cu(II) 2p XPS and XAS.[39,47,48,50]

In all Cu(II) K-edges included in this study, this pair of transitions occurs such that the apparent ratio of their intensities, $I_{1s \rightarrow 4p}/I_{1s \rightarrow 4p+shakedown}$, ($I_{main}/I_{shakedown}$) is close to or greater than 1.[51] However, in the Cu(III) edges, the 1s → 4p + shakedown transition is dramatically enhanced in intensity, while the 1s → 4p transition is diminished (i.e., $I_{main}/I_{shakedown} < 1$) (Figure 4). This effect is most easily observed in second derivative spectra, where the positions of peaks are more pronounced against the smooth background absorption. Similar redistributions in the relative intensities of main and satellite peaks with changing oxidation state have been observed in 2p XPS of solid-state copper oxides (for example, $Cu^{II}O$ and $NaCu^{III}O_2$).[52−54] In addition, the energy separation of the 1s → 4p and 1s → 4p + shakedown transitions (represented by the variable *W*) is greater for the Cu(III) complexes than for the corresponding Cu(II) complexes. Again, the same trend has been observed in the main/satellite peak splitting in 2p XPS for the solid copper oxides. Both trends are most apparent in the K-edges for the square-planar complexes $[Cu^{III}_2(\mu\text{-}O)_2(L_{ME})_2]^{2+}$ and $[Cu^{II}_2(\mu\text{-}OH)_2(L_{ME})_2]^{2+}$, where the 1s → 4p and 1s → 4p + shakedown transitions are fairly well resolved above the background of the rising edge absorption. The discrete nature of these complexes eliminates potential complications from long-range effects observed in spectra for some solid-state materials. An analysis was therefore carried out to interpret the observed differences in $I_{main}/I_{shakedown}$ and *W* for these two K-edges.

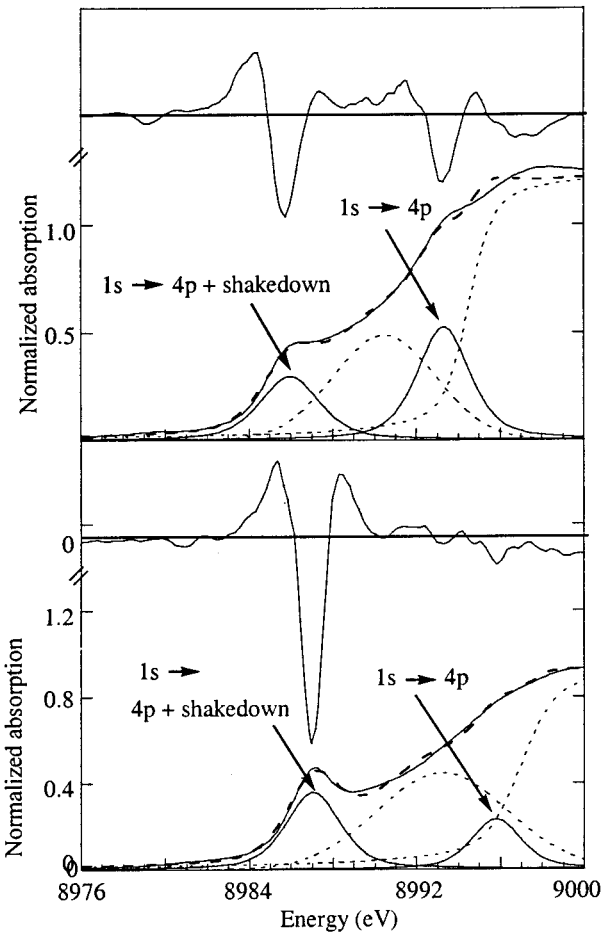

Figure 4. Results of fits to K-edge data for $[Cu^{II}_2(\mu\text{-}OH)_2(L_{ME})_2]^{2+}$ (top) and $[Cu^{III}_2(\mu\text{-}O)_2(L_{ME})_2]^{2+}$ (bottom). Data are shown as solid lines, and fits to the data as heavy dashed lines. Each fit is the sum of three peaks and one arctangent curve shown. Peak assignments are as shown on the plots. Second derivatives of the data (weighted × 3) are plotted over each spectrum. Peak positions are clearly visible in the second derivative spectra.

The measured energy separation between each pair of peaks and their intensity ratio can be used as empirical observables in a configuration interaction (CI) based model developed by Sawatsky and co-workers.[55−57] According to this model, the ground state of a given Cu(II) complex can be described as an admixture of two contributing configurations, $|3d^9\rangle$ and $|3d^{10}\underline{L}\rangle$ ($\underline{L}$ = a hole in the ligand valence p shell):

(50) Note the naming convention for Cu(II) 2p XPS peaks: the larger *main* peak is attributed to the $|\underline{2p}3d^{10}\underline{L}\rangle$ shakedown final state, while the smaller satellite peak to higher energy is attributed to the $|\underline{2p}3d^9\rangle$ unrelaxed final state.

(51) Such an intensity distribution was also typical of the range of Cu(II) K-edges included in ref 27.

(52) Mizokawa, T.; Fujimori, A.; Namatame, H.; Akeyama, K.; Kosugi, N. *Phys. Rev. B* **1994**, *49*, 7193−7203.

(53) Mizokawa, T.; Namtame, H.; Fujimori, A.; Akeyama, K.; Kondoh, H.; Kuroda, H.; Kosugi, N. *Phys. Rev. Lett.* **1991**, *67*, 1638−1641.

(54) Steiner, P.; Kinsinger, V.; Sander, I.; Siegwart, B.; Hufner, S.; Politis, C.; Hoppe, R.; Müller, H. P. *Z. Phys. B* **1987**, *67*, 497−502.

(55) van der Laan, G.; Westra, C.; Haas, C.; Sawatsky, G. A. *Phys. Rev. B* **1981**, *23*, 43−69.

(56) Zaanen, J.; Sawatsky, G. A.; Allen, J. W. *Phys. Rev. Lett.* **1985**, *55*, 418−421.

(57) Zaanen, J.; Sawatsky, G. A. *Phys. Rev. B* **1986**, *33*, 8074−8083.

$$\Psi_g(Cu^{II}) = \cos\Theta|3d^9\rangle - \sin\Theta|3d^{10}\underline{L}\rangle$$

These two configurations are separated by an energy Δ in the ground state before configurational interaction, such that $\Delta = \langle 3d^{10}\underline{L}|H|3d^{10}\underline{L}\rangle - \langle 3d^9|H|3d^9\rangle$. Δ is therefore related to the energy required for the $|3d^n\rangle \rightarrow |3d^{n+1}\underline{L}\rangle$ transition, the charge-transfer energy. The mixing, or covalent interaction, of the two configurations in the ground state is described by the transfer integral, $T = \langle 3d^{10}\underline{L}|H|3d^9\rangle$. Thus ground-state covalency is modeled as the mixing of the charge-transfer $|3d^{10}\underline{L}\rangle$ state into the $|3d^9\rangle$ state. By analogy, the ground state of a given Cu(III) complex is described as a mixture of two contributing states, $|3d^8\rangle$ and $|3d^9\underline{L}\rangle$:

$$\Psi_g(Cu(III)) = \cos\Theta|3d^8\rangle - \sin\Theta|3d^9\underline{L}\rangle$$

Here $\Delta = \langle 3d^9\underline{L}|H|3d^9\underline{L}\rangle - \langle 3d^8|H|3d^8\rangle$, and $T = \langle 3d^9\underline{L}|H|3d^8\rangle$.

Excitation of the 1s $\rightarrow$ 4p transition can occur with two possible final states, corresponding to the previously described main and shakedown peaks in the Cu K-edge. For the Cu^{II} case, these are

$$\Psi_{main(1s\rightarrow 4p)}(Cu^{II}) = \sin\Theta'|\underline{1s}3d^9\rangle + \cos\Theta'|\underline{1s}3d^{10}\underline{L}\rangle$$

$$\Psi_{shakedown(1s\rightarrow 4p+shakedown)}(Cu^{II}) = \cos\Theta'|\underline{1s}3d^9\rangle - \sin\Theta'|\underline{1s}3d^{10}\underline{L}\rangle$$

As stated previously, the main peak arises from transitions to a final state of largely $|\underline{1s}3d^9\rangle$ character, while the shakedown peak arises from transitions to a mainly $|\underline{1s}3d^{10}\underline{L}\rangle$ excited state. The Cu(III) case is constructed similarly:

$$\Psi_{main(1s\rightarrow 4p)}(Cu(III)) = \sin\Theta'|\underline{1s}3d^8\rangle + \cos\Theta'|\underline{1s}3d^9\underline{L}\rangle$$

$$\Psi_{shakedown(1s\rightarrow 4p+shakedown)}(Cu(III)) = \cos\Theta'|\underline{1s}3d^8\rangle - \sin\Theta'|\underline{1s}3d^9\underline{L}\rangle$$

The value of Θ is restricted such that $0° < \Theta < 90°$. It follows that for $\Delta > 0$, $0° < \Theta < 45°$, and for $\Delta < 0$, $45° < \Theta < 90°$. Then for $\Delta - Q < 0$, $45° < \Theta' < 90°$, and for $\Delta - Q > 0$, $0° < \Theta' < 45°$.[55]

The energy matrix for describing the excited state is similar to that for the ground state, with the addition of a term, Q, such that $\Delta - Q_{Cu(II)} = \langle \underline{1s}3d^9|H|\underline{1s}3d^9\rangle$ and $\Delta - Q_{Cu(III)} = \langle \underline{1s}3d^8|H|\underline{1s}3d^8\rangle$. Q is an atomic parameter equal to the core-hole/valence-electronic Coulomb interaction. It describes the degree of relaxation of the valence electron configuration accompanying the creation of a core hole. For a metal with the same ligand set, it is expected to increase with increasing charge on the absorbing metal (Figure 5).

These ground and excited state parameters are related to the previously described experimental observables, W and $I_{main}/I_{shakedown}$, by the following four expressions:

$$\tan(2\Theta) = 2T/\Delta \quad (1)$$

$$\tan(2\Theta') = 2T/(\Delta - Q) \quad (2)$$

$$W = [(\Delta - Q)^2 + 4T^2]^{1/2} \quad (3)$$

$$\frac{I_{main}}{I_{shakedown}} = \left(\frac{\sin\Theta'\cos\Theta - \cos\Theta'\sin\Theta}{\cos\Theta'\cos\Theta - \sin\Theta'\sin\Theta}\right)^2 = \tan^2(\Theta' - \Theta) \quad (4)$$

The model is completely described by these equations and the seven parameters just outlined. Three of these refer to the ground-state metal−ligand interaction (Δ, T, and Θ), two to the excited state and the effect of the 1s core hole in the excited state (Q and Θ'), and two to experimental observables (W and $I_{main}/I_{shakedown}$).

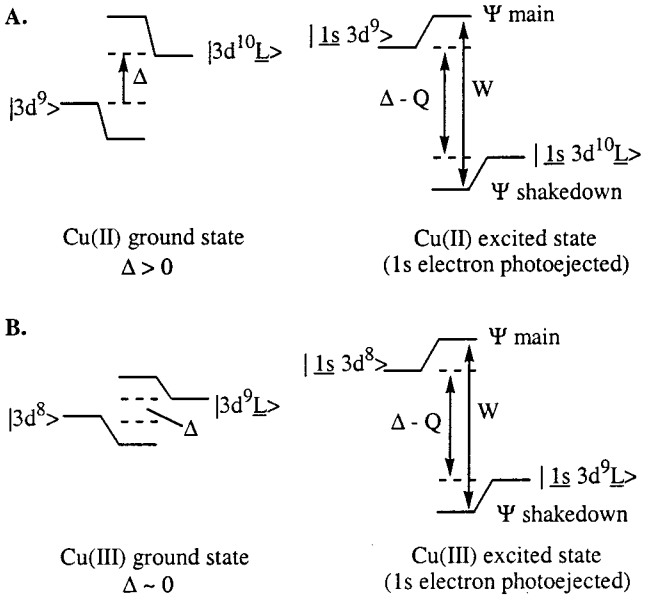

Figure 5. Diagrams of the ground and excited states for (A) Cu(II) and (B) Cu(III), using the parameters of the CI model.

Typically, W and $I_{main}/I_{shakedown}$ are measured directly from spectra (K-edge or 2p XPS, e.g.) and a third parameter from the model is determined by some other means. Equations 1−4 can then be solved to determine the remaining four unknowns. A prior 2p XPS study of D_{2d} $CuCl_4^{2-}$ was performed similarly, with $I_{main}/I_{shakedown}$ and W measured from the spectrum, Q set to a value determined to be valid for Cu(II), and T, Δ, Θ, and Θ' obtained from simultaneous solution of eqs 1−4. Parameter values determined from this XPS study for D_{2d} $CuCl_4^{2-}$ included the following: $\Delta = 0.88$ eV, $Q = -8.9$ eV, and $T = 1.5$ eV.[58] K-edge data for D_{2d} $CuCl_4^{2-}$ were analogously analyzed in a previous study.[39] Though z-polarized data were used, it was still not possible to simulate the background rising edge absorption with precision. Measured peak intensities were imprecise as a consequence, and $I_{main}/I_{shakedown}$ was therefore treated as an unknown quantity. The values of Δ and T obtained from the 2p XPS study were used directly, with the measured value of W, to solve eqs 1−4 for the remaining four parameters (Q(1s/3d), Θ, Θ', and $I_{main}/I_{shakedown}$). The calculated $I_{main}/I_{shakedown}$ of ~0.7, as anticipated, differed somewhat from the measured estimate of ~1.2. It was also found that Q(1s/3d) = 6.8 eV, while the 2p XPS study yielded a larger value, Q(2p/3d) = 8.9 eV. Note that Q, which describes the Coulombic attraction of the valence electrons and core hole, is expected to be smaller for the 1s/3d interaction due to greater shielding of a 1s core hole relative to a 2p hole. By contrast, Δ and T relate to the ground state of the molecule and are not expected to depend on the type of measurement used to obtain them.

An approach similar to the one used in analyzing $CuCl_4^{2-}$ K-edge data was used in the analysis of the K-edges for $[Cu^{II}_2(\mu\text{-}OH)_2(L_{ME})_2]^{2+}$ and $[Cu^{III}_2(\mu\text{-}O)_2(L_{ME})_2]^{2+}$. Ground-state parameters Δ and T were derived from previous XPS and XAS studies on related materials, and W was measured from data.

(58) Gewirth, A. A.; Cohen, S. L.; Schugar, H. J.; Solomon, E. I. *Inorg. Chem.* **1987**, *26*, 1133−1146.

Table 3. Parameter Values Used and Results of CI-Model Calculation for $[Cu^{II}_2(\mu\text{-}OH)_2(L_{ME})_2]^{2+}$ and $[Cu^{III}_2(\mu\text{-}O)_2(L_{ME})_2]^{2+}$

parameter	$[Cu^{II}_2(\mu\text{-}OH)_2(L_{ME})_2]^{2+}$	$[Cu^{III}_2(\mu\text{-}O)_2(L_{ME})_2]^{2+}$
Δ, eV	1.5	0.7
T, eV	1.4	2.3
Q, eV	8.2	8.2
$\cos^2\Theta'$, %	3.82	7.37
$\cos^2\Theta$, %	73.6	57.5
W, eV	7.3	8.8
$I_{main}/I_{shakedown}$		
predicted	1.22	0.44
measured[a]	1.59	0.636

[a] Peak intensities calculated as measured height × fwhm; see Table 2.

$I_{main}/I_{shakedown}$, Θ, Θ', and Q were then computed through simultaneous solution of eqs 1−4. Calculated values of $I_{main}/I_{shakedown}$ were compared with those estimated from data. T and Δ for $[Cu^{II}_2(\mu\text{-}OH)_2(L_{ME})_2]^{2+}$ were determined as follows. The average value of Δ previously determined from analysis of 2p XPS for CuO was used ($\Delta \sim 1.5$ eV).[59] This value is larger than that determined for $CuCl_4^{2-}$, consistent with the reduced covalency of the hydroxide ligands, relative to chloride. Similarly, as T is proportional to metal/ligand overlap, $T_{\{Cu(II)_2(\mu-OH)_2\}^{2+}}$ is expected to be slightly smaller than $T_{CuCl_4^{2-}}$ (1.5 eV); a value of ~1.4 eV reproduced the data well and was therefore used. Solving eqs 1−4, using $\Delta = 1.5$ eV, $T = 1.4$ eV, and $W = 7.3$ eV as input, produced a set of predicted values for Θ, Θ', W, and $I_{main}/I_{shakedown}$ (Table 3). The calculated value of $Q = 8.2$ eV is 1.4 eV larger than that obtained from K-edge measurements on $CuCl_4^{2-}$. This may be due to the greater nephalauextic effect of chloride versus hydroxide ligands, and is consistent with previously documented trends in Q.[60] The calculated $I_{main}/I_{shakedown}$ was comparable in magnitude to the empirically estimated values. The median ground state percent d-character ($\cos^2\Theta$) resulting from the calculation was ~75%, larger than the value previously obtained for $CuCl_4^{2-}$ (64%), again as might be expected for a molecule with amine and hydroxide ligands (Table 3).

For analysis of the $[Cu^{III}_2(\mu\text{-}O)_2(L_{ME})_2]^{2+}$ edge, $W = 8.8$ eV was measured from fits to the spectrum (Table 2). Values of Δ and T were derived from prior CI-model analyses of the 2p photoelectron and absorption spectra for $NaCu^{III}O_2$ and $La_2Li_{0.5}Cu^{III}_{0.5}O_4$, respectively.[52,59] Parameters obtained from analyses of the main/satellite peaks in 2p XPS or 2p XAS (L-edge) data included the following: $\Delta = -1 \pm 1$ eV, $Q = 10$ eV, $T = 2.9$ eV (XPS);[52] and $\Delta = -1.9$ eV, $T_{B1g} = 1.73$ eV (XAS).[59] A negative value for Δ implies that the $|3d^9\underline{L}\rangle$ configuration is lower in energy than the $|3d^8\rangle$ configuration in the ground state, while the large values for T suggest the ground state is a highly covalent mixture of these configurations. A more general trend in values of T and Δ for the Cu(II) and Cu(III) oxides is also evident, and consistent with chemical expectation: $\Delta_{Cu(III)} < \Delta_{Cu(II)}$ and $T_{Cu(III)} > T_{Cu(II)}$. Similar oxidation-state dependent trends in T and Δ have been documented in analyses of 2p XPS data of other materials, e.g., $Fe^{II}/Fe^{III}/Fe^{IV}$ and $Mn^{II}/Mn^{III}/Mn^{IV}$ oxides.[61,62] These trends for T and Δ are important for predicting oxidation-state-dependent trends in the remaining four parameters of the model. The average of the two values for T ($T = 2.3$ eV) was used in solving eqs 1−4. A range of small negative and positive values for Δ were also used as input, and the equations were solved for $I_{main}/I_{shakedown}$, Q, Θ, and Θ' (Figure 6). Small values of Δ reproduced the observed trend of the smaller $I_{main}/I_{shakedown}$ ratio for Cu(III). However, only positive values of Δ yielded $Q_{Cu(III)} \geq Q_{Cu(II)}$. Work on the 2p XPS of iron and manganese oxides suggests that Q should stay the same or increase with increasing metal oxidation state, assuming the ligands around the metal are similar.[62,63] The smallest value of Δ for which this is true is $\Delta \sim 0.7$ eV. Using $T = 2.3$ eV, $\Delta = 0.7$ eV, and $W = 8.8$ eV, the model predicts a median ground-state d-character of ~57%, consistent with the description of $\{Cu^{III}_2(\mu\text{-}O^{2-})_2\}^{2+}$ as a largely covalent Cu(III) site but possibly a lower bound (vide infra).

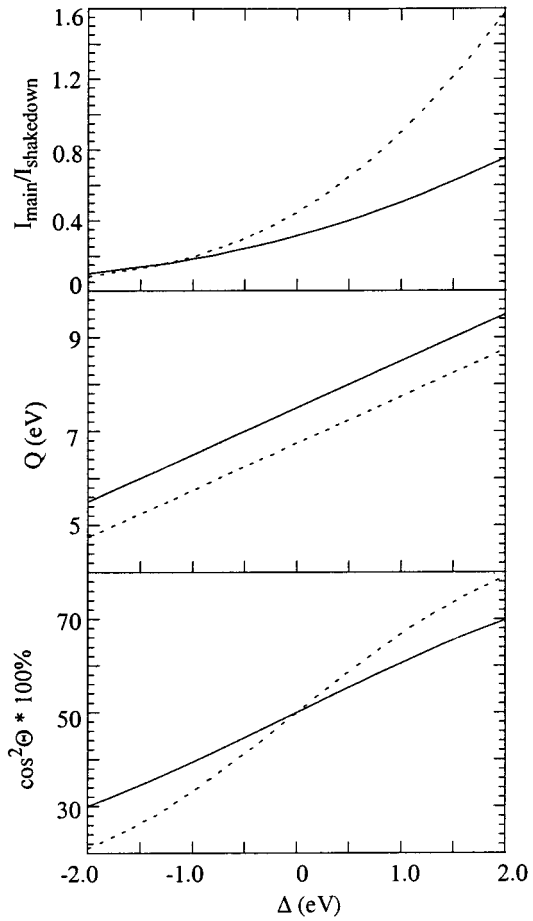

Figure 6. Plots of calculated $I_{main}/I_{satellite}$, Q, and $\cos^2\Theta$, showing how each varies with changing values of Δ. Solid lines were calculated from eqs 1−4 using parameters for $[Cu^{III}_2(\mu\text{-}O)_2(L_{ME})_2]^{2+}$ ($W = 8.8$ eV and $T = 2.3$ eV). Dotted lines were calculated using parameters for $[Cu^{II}_2(\mu\text{-}OH)_2(L_{ME})_2]^{2+}$ ($W = 7.3$ eV and $T = 1.4$ eV).

Mixed-Valence Species. The Cu K-edge for the mixed-valence complex (type II localized in the solid state) $[Cu^{II}Cu^{III}O_2(L_{TM})_3]^{3+}$ (L_{TM} = *N,N,N′,N′*-tetramethyl-*trans*-(1*R*,2*R*)-

(59) Hu, Z.; Kaindl, G.; Warda, S. A.; Reinen, D.; de Groot, F. M. F.; Müller, B. G. *Chem. Phys.* **1998**, *232*, 63−74.

(60) For example, similar variations in Q have been observed in analyses of 2p XPS spectra for $KFe^{III}S_2$ ($|Q| = 3.6$) and $[Fe^{III}Cl_4]^-$ ($|Q| = 4.4$). Differences in Q were rationalized as being due to the greater nephalauxetic effect of Cl^- versus S^{2-} (Rose, K.; Shadle, S. E.; Glaser, T.; de Vries, S.; Cherepanov, A.; Canters, G. W.; Hedman, B.; Hodgson, K. O.; Solomon, E. I. *J. Am. Chem. Soc.* **1999**, *121*, 2353−2363). See ref 63 for further examples.

(61) Bocquet, A. E.; Fujimori, A.; Mizokawa, T.; Saitoh, T.; Namatame, H.; Suga, S.; Kimizuka, N.; Takeda, Y.; Takano, M. *Phys. Rev. B* **1992**, *45*, 1561−1570.

(62) Bocquet, A. E.; Mizokawa, T.; Saitoh, T.; Namatame, H.; Fujimori, A. *Phys. Rev. B* **1992**, *46*, 3771−3780.

(63) For $Fe^{II}O$, $Fe^{III}_2O_3$, and $SrFe^{IV}O_3$, $Q = 8.4$, 8.4, and 9.4 eV, respectively. Values obtained for Δ for this series also follow the expected oxidation state trend: 6.0, 3.5, and 0 eV for the Fe(II), Fe(III), and Fe(IV) oxides, respectively. The Mn oxides $Mn^{II}O$, $LaMn^{III}O_3$, and $SrMn^{IV}O_3$ follow similar trends. For the series $Q = 8.4$, 9.0, and 9.4 eV and $\Delta = 6.5$, 4.5, and 2.0 eV see ref 62 and references therein.

cyclohexane diamine)[30] was measured. Each copper center in this complex, taken on its own, is structurally and electronically similar to one of the copper centers in the dimeric complexes, $[Cu^{III}_2(\mu\text{-}O)_2(L_{ME})_2]^{2+}$ or $[Cu^{II}_2(\mu\text{-}OH)_2(L_{ME})_2]^{2+}$. Each of the coppers in both the trinuclear and dimeric species are ligated in a square-planar array, with a very similar bidentate diamine ligand and two oxo or hydroxo bridging ligands (Scheme 1). The edge shape is highly dependent on the local environment of the absorbing metal. The edge spectrum for the trinuclear complex should therefore be approximated by a sum of the edges for these dimeric complexes, taken in a ratio of 1 $[Cu^{III}_2(\mu\text{-}O)_2(L_{ME})_2]^{2+}$:2 $[Cu^{II}_2(\mu\text{-}OH)_2(L_{ME})_2]^{2+}$. The product spectrum resulting from a weighted addition of these two edges closely reproduces edge data for $[Cu^{II}_2Cu^{III}O_2(L_{TM})_3]^{3+}$ (Figure 7B). It is also notable to compare edges for the trinuclear complex with those of the two dimers (Figure 7A). The edge for the trinuclear complex is energy shifted relative to the edge for $[Cu^{II}_2(\mu\text{-}OH)_2(L_{ME})_2]^{2+}$, though only slightly. The preedge does not show two well-resolved peaks at ~8979 and 8981 eV, but rather appears as a flattened absorption across this energy range (Figure 7A, inset); similarly, there are not two transitions visible in the 1s → 4p energy region. Second derivative spectra, however, show that the intense 1s → 4p + shakedown transition is split, with peaks appearing at the respective energies of the individual 1s → 4p + shakedown transitions of the two dimers (Figure 7C).[64]

Cu^{II}-O-R Results. Cu K-edges were measured for $[Cu^{II}BDB]$ and its one-electron oxidized form $[Cu^{II}\text{-}\underline{O}\text{-}BDB]^+$ ($\underline{O}$ = a ligand hole based on a coordinating phenolate oxygen; $[Cu^{II}BDB]$ = [*N*,*N*′-bis[2,4-(di-*tert*-butyl)salicylidene]-2,2-(1,1′-binaphthylene)-diiminato]Cu(II)][65] (Figure 8, Scheme 1). $[Cu^{II}\text{-}\underline{O}\text{-}BDB]^+$ is an EPR-silent species, for which the Zn^{2+} analogue gives a strong radical signal in EPR measurements. $1e^-$-oxidized, phenolate-containing fragments of the ligand yield identical radical signals. The Cu(II) complex, when oxidized by $1e^-$, is EPR silent. It was concluded that $[Cu^{II}\text{-}\underline{O}\text{-}BDB]^+$ is formally a $d^9Cu^{II}\text{-}\underline{L}$ species, where $\underline{L}$ designates a coordinated oxidized ligand. The unpaired ligand-based electron antiferromagnetically couples to the unpaired Cu(II) electron, forming a diamagnetic, EPR-silent species (at both 77 and 4 K).[11,12,66]

Edges for these species (Figure 8) demonstrate that the charge on the copper remains apparently unchanged as the complex is oxidized. Neither the edge nor preedge for $[Cu^{II}\text{-}\underline{O}\text{-}BDB]^+$ is energy shifted, relative to the edge for $[Cu^{II}BDB]$. In fact, the 1s → 4p region of the edge for the more oxidized complex appears shifted to slightly *lower* energy. This may actually be due to a shift in the absorption maximum of the edge to lower energy. As the maximum is likely a MS peak due to backscattering from first-coordination shell ligands,[49] such a shift may be expected to accompany a general elongation of first-coordination shell Cu−ligand distances. EXAFS analysis has elucidated structural changes that occur with one-electron oxidation of $[Cu^{II}BDB]$: slight expansion of the first coordination sphere and the acquisition of a fifth ligand to the copper (presumably coordination of the BF_4^- counteranion).[14,67] These structural changes may account for the observed changes in edge shape and the energy shift of the first MS peak.

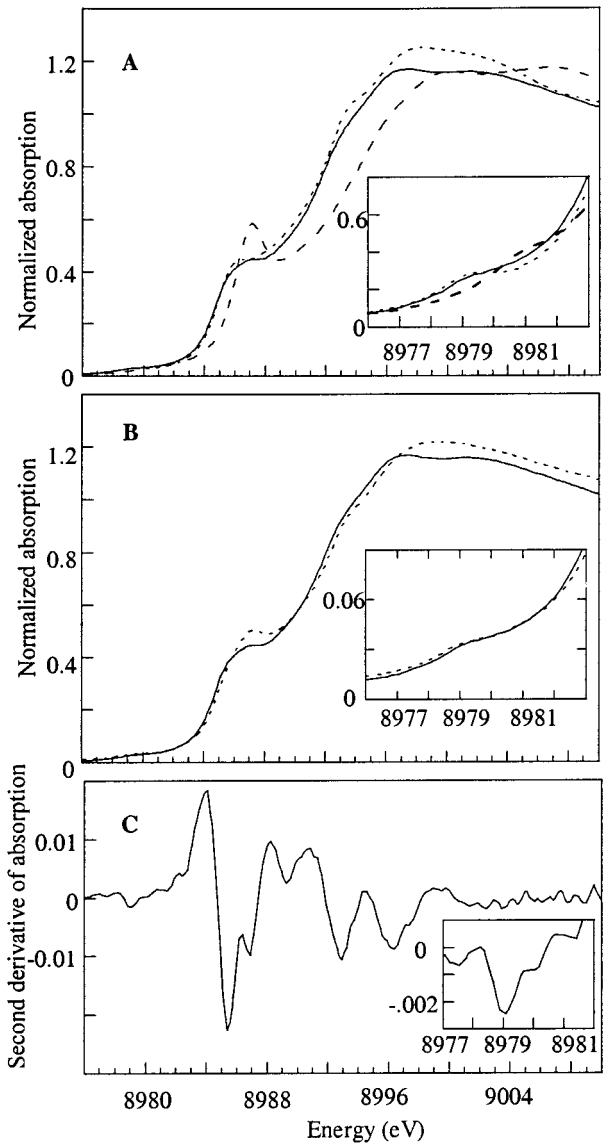

Figure 7. K-edge data for the trinuclear complex $[Cu^{II}Cu^{II}Cu^{III}O_2(L_{TM})_3]^{2+}$. (A) Trinuclear data (solid line) shown with data for $[Cu^{II}_2(\mu\text{-}OH)_2(L_{ME})_2]^{2+}$ (dotted line) and $[Cu^{III}_2(\mu\text{-}O)_2(L_{ME})_2]^{2+}$ (dashed line). The inset shows the amplified preedge (1s → 3d transition) region (8976−8983 eV). The edge for the trinuclear complex is only slightly energy-shifted relative to the edge for the Cu(II) dimer. The 1s → 3d transitions for the Cu(II) and Cu(III) dimers are discrete peaks at 8979 and 8981 eV, respectively, while the transition for the trinuclear appears as a broad plateau over both these energies. (B) Trinuclear data (solid line) shown with the result of adding together edge data for $[Cu^{II}_2(\mu\text{-}OH)_2(L_{ME})_2]^{2+}$ and $[Cu^{III}_2(\mu\text{-}O)_2(L_{ME})_2]^{2+}$, in a 1:2 ratio. Preedge regions are shown in the inset. Note the striking similarity of the trinuclear data to the simulated edge. (C) Second derivative of the edge data for the trinuclear complex. Two peaks are visible in the 1s → 4p + shakedown region, at ~8985 and 8987 eV, the respective energies of the 1s → 4p + shakedown transition for $[Cu^{II}_2(\mu\text{-}OH)_2(L_{ME})_2]^{2+}$ and $[Cu^{III}_2(\mu\text{-}O)_2(L_{ME})_2]^{2+}$. The second derivative of the preedge region is shown in the inset. Instead of a single peak, a peak with a shoulder is observed.

Effect of Short Cu−L Bonds. Finally, to examine the effects of short, Cu(III)-like bonds on the 1s → 3d transition energy, the Cu K-edge for $Cu^{II}(OC_6H_4\text{-}p\text{-}F)(HB(3,5\text{-}{}^i Pr_2pz)_3)$ was measured (see Supporting Information). The X-ray crystal structure for this complex features a 1.729(7) Å $Cu-O_{phenolate}$ bond.[67] This is remarkably short for a Cu(II) complex, but is within the range of observed copper−oxygen bond distances

(64) Because of the extreme temperature sensitivity of the complex, it was important to demonstrate that the trinuclear sample on which the edge was measured was intact. To this end, the EXAFS for the trinuclear cluster was fit, with good agreement between the EXAFS results and crystallographic structure. Both short Cu(III)−ligand and longer Cu(II)−ligand distances were determined.

(65) Wollmann, R. G.; Hendrickson, D. N. *Inorg. Chem.* **1977**, *16*, 732−733.

(66) Wang, Y. Ph.D. Thesis, Stanford University, 1999.

(67) Kitajima, N.; Katayama, T.; Fujisawa, K.; Iwata, Y.; Moro-oka, Y. *J. Am. Chem. Soc.* **1993**, *115*, 7872−7873.

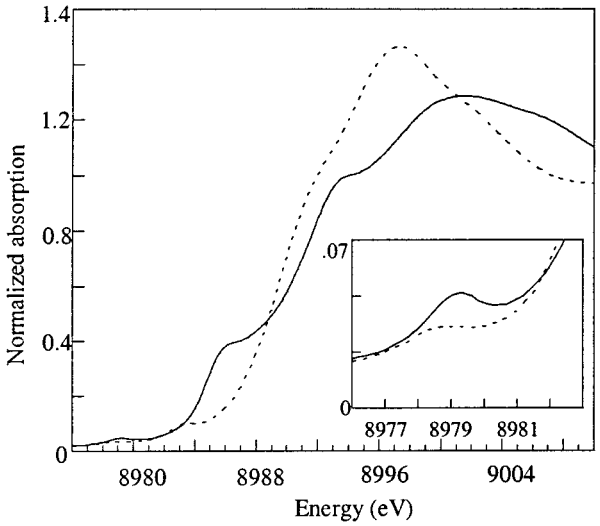

Figure 8. Cu K-edges for [Cu^{II}BDB] (dotted line) and 1e$^-$-oxidized [Cu^{II}-O-BDB]$^+$ (solid line). Preedge regions (1s → 3d transitions) are shown amplified in the inset. The edge for the more oxidized complex is not energy shifted. The preedges for both complexes show peaks at ~8979.5 eV. Oxidation of the complex does not appear to affect the 1s electron binding energy.

for Cu(III). On this basis, the oxidation state of the copper might be assigned as +3. However, the complex is paramagnetic as shown by EPR. Consistent with this observation, the 1s → 3d transition for this complex appears at 8978.2 eV, an energy value at the low end of the range expected for a Cu(II) complex.

Discussion

Cu(II)/Cu(III) Pairs. Ligand environment, coordination geometry, and oxidation state all strongly influence the appearance of transition metal K-edges.[43−45,68] The ligand environment and geometry of the compounds in each pair presented in Figure 1 are the same or as similar as possible; however, one compound of each pair is oxidized by 1e$^-$ (i.e., per copper) relative to the other (Scheme 1). In each case, one compound contains Cu(II), while the copper in the oxidized compound is Cu(III). The Cu(III) assignments are structurally and spectroscopically consistent: the copper−oxygen bond lengths in these compounds are remarkably short (Cu−O ~1.76−1.85 Å) relative to typical Cu(II)−ligand bonds (Cu−O ~1.9−2.0 Å), and the compounds are EPR silent (77 K). Each of these observations is consistent with the increased charge and formally d^8 nature of Cu(III), though neither is a direct or unambiguous consequence of the copper oxidation state. Examples of paramagnetic Cu(III) and diamagnetic Cu(II) species are known, the latter being especially common due to antiferromagnetic coupling of the unpaired copper spin with another nearby electron spin;[13,20,69] likewise, several well-characterized Cu(II) species with unusually short Cu−ligand bond distances exist.[67,70] Structural or magnetic indicators of oxidation state are therefore potentially misleading. High-energy spectroscopy has traditionally been useful for probing metal oxidation state, as it accesses largely unshielded, core electrons, and therefore the quantity most fundamental to oxidation state: the effective nuclear charge on the metal.

Cu K-edges for each of the same-ligand, Cu(II)/Cu(III) pairs of compounds exhibit a shift to higher energy of the entire edge for the Cu(III) species, relative to the edge for the Cu(II) species (Figure 1). Similar shifts in the edge with changing oxidation state are also seen in other transition metals.[43,44,68] Such a shift is expected and reflects the increased effective nuclear charge of Cu(III) relative to Cu(II). A greater effective nuclear charge gives rise to higher binding energies for core electrons, and therefore greater bound-state transition and photoejection energies. As indicated above, the effect of the increased effective nuclear charge on binding energies should be felt most strongly by the core electrons. However, as it is not possible to infer 1s binding energies directly from the complicated structure of the K-edge, identifying oxidation states from these edges requires some systematic analysis of edge structure.

All of the Cu(II) edges have the same set of transitions. These have their apparent counterparts in the Cu(III) edges (Figure 1). No new transitions unique to the Cu(III) edges are observed. In general, the magnitude of the observed Cu(III) energy shift in the edge is fairly small and not consistent from point to point along the edge (~0−2 eV). Such energy shifts between analogous features in Cu(II) and Cu(III) K-edges are only strictly observed when the compounds compared have the *same/highly similar* ligands (Figure 1). Energy shifts between individual features may or may not be observed if the two compounds have *different* ligands (Figure 2). This observation reflects the fact that the absolute energies of several edge features (e.g., the first inflection point of the edge, the 1s → 4p transition, 1s → 4p + shakedown transition, principal maximum of the edge) are not wholly functions of the metal oxidation state. Hence energies for these features vary broadly for complexes with the same oxidation state but with different ligands (Figure 2). Ligand effects such as covalency are known to influence the energy positions of the 1s → 4p and 1s → 4p + shakedown transitions (vide supra),[39] while geometric structure may dictate the energy position of the edge absorption maximum.[29,49] The energy of the first inflection point along the edge is biased by the presence of the 1s → 4p + shakedown transition along the same portion of the edge. Thus none of these features can be used unambiguously as a marker of oxidation state.

Preedge. At least one point of consistency exists across each of the sets of Cu(II) and Cu(III) edges, which distinguishes the two. In a previous study including Cu K-edges for 40 different Cu(II) compounds, a preedge feature—a weak, electric dipole-forbidden ($\Delta l \neq \pm 1$) but quadrupole-allowed 1s → 3d transition—appeared consistently at ~8979 eV (8978.8 ± 0.4 eV).[29] This consistency persisted over a broad range of Cu(II) coordination geometries and ligand types. Preedges for the Cu(II) compounds included in the present work also appear in this energy range. Ligand field effects are thought to account for much of the observed range (≤1 eV) of Cu(II) preedge energies. For example, the 1s → 3d transition for tetrahedrally distorted (D_{2d}) [Cu^{II}Cl$_4$]$^{2-}$ is an intense peak centered at ~8978.4 eV. The transition for the D_{4h} isomer is a smaller peak centered about 0.4−0.5 eV to higher energy.[71] The energy shift in these transitions illustrates the effect of a change in ligand field on the 1s → 3d energy (i.e., weak field D_{2d} to stronger field D_{4h}), in the absence of other perturbations.

(68) Westre, T. E.; Kennepohl, P.; DeWitt, J. G.; Hedman, B.; Hodgson, K. O.; Solomon, E. I. *J. Am. Chem. Soc.* **1997**, *119*, 6297−6314.

(69) Cole, J. L.; Tan, G. O.; Yang, E. K.; Hodgson, K. O.; Solomon, E. I. *J. Am. Chem. Soc.* **1990**, *112*, 2243−2249.

(70) For example: (a) McMullen, A. K.; Tilley, D.; Rheingold, A. L.; Geib, S. J. *Inorg. Chem.* **1989**, *28*, 3772−3774. (b) Colacio, E.; Costes, J.-P.; Kivekas, R.; Laurent, J.-P.; Ruiz, J. *Inorg. Chem.* **1990**, *29*, 4240−4246. (c) Butcher, R. J.; O'Connor, C. J.; Sinn, E. *Inorg. Chem.* **1981**, *20*, 537−545. (d) Atkins, R.; Brewer, G.; Kokot, E.; Mockler, G. M.; Sinn, E. *Inorg. Chem.* **1985**, *24*, 127−134. (e) Jacobson, R. R.; Tyeklár, A.; Farooq, A.; Karlin, K. D.; Liu, S.; Zubieta, J. *J. Am. Chem. Soc.* **1988**, *110*, 3690−3692. (f) Lee, S.; Holm, R. H. *J. Am. Chem. Soc.* **1993**, *115*, 11789−11798.

(71) K. O. Hodgson, unpublished results.

1s → 3d transition energies for the Cu(III) compounds reported here likewise cluster around a common, but higher, energy value: 8981 ± 0.5 eV. This ~2 eV shift to higher energy sets the Cu(III) 1s → 3d transition outside of the energy range found for the Cu(II) complexes (Figure 3). Because the Cu(III) and Cu(II) preedge features are distinct in energy, the energy position of this transition may offer the best means of analytically identifying Cu(III), *without* reference to the edge for an exact counterpart Cu(II) compound. This is especially important as the appropriate reference compound may not exist or may not be easily obtained (e.g., in the case of a trapped reaction intermediate). Also, comparisons based on other features of a given Cu(III) edge and the edge for a differently liganded Cu(II) complex are potentially problematic, for reasons described above.

The raised energy of the preedge feature may be interpreted as being largely due to greater effective nuclear charge exerted by the Cu(III) on the tightly bound 1s electron. It is interesting to note the magnitude of the Cu(II)/Cu(III) preedge shift in light of at least one reported ab initio calculation of 1s ionization energies for the following series: Cu^{I}_2O, $Cu^{II}O$, and $KCu^{III}O_2$ (using a self-consistent-field discrete-variational Xα approach, and the transition-state method). The *relative* 1s ionization potentials calculated for this series were $\Delta(Cu^{II}O/Cu_2{}^{I}O) = 1.7$ eV and $\Delta(KCu^{III}O_2/Cu^{II}O) = 2.1$ eV.[72] The 2.1 eV shift between 1s ionization potentials for the Cu(II) and Cu(III) oxides is comparable to the ~2 eV shift observed between the Cu(II) and Cu(III) preedges. This suggests that, at this level of theory, much of the ~2 eV Cu(II)/Cu(III) preedge energy shift may be associated with the increased binding energy of the 1s electron in Cu(III). Other ligand-defined effects are also expected to contribute to the preedge energy shift. Cu(III) should be subject to greater ligand field splitting than Cu(II), given the same ligand set. This would raise the energy of the acceptor orbital of the transition (antibonding $3d_{x^2-y^2}$), increasing the overall energy of the Cu(III) 1s → 3d transition. Ligand field effects are expected to be a secondary perturbation, e.g., producing the range of preedge energies for Cu(II) complexes with different ligands (±0.4 eV) and for Cu(III) (±0.5 eV). These effects in turn are small in comparison to the ~2 eV shift in the 1s → 3d transition.

The preedge transition as a marker of oxidation state has the advantage of being a bound state transition (1s → 3d) that exists as a *discrete peak*, separated from the complicated structure of the rising edge. Its exact energy and approximate intensity are simple to assess. The transition is also not complicated by relaxation effects resulting from photoemission processes. Preedge energy has been shown to correlate with oxidation state for a number of transition metals (e.g., Ni, Mn, Fe, and V).[43,44,68,73] In these cases, the observed shifts in preedge energy with changes in oxidation state are comparable in order of magnitude to that observed for Cu(II)/Cu(III): 1−2 eV per unit oxidation.

1s → 4p Transitions: Shakedown Contributions and Covalency. The 1s → 4p (shakedown) and 1s → 4p (main) transitions in the Cu(II)/Cu(III) pairs of edges follow two general oxidation-state dependent trends: the energy separation between these peaks (*W*) is greater in the Cu(III) complexes, and the pattern of intense-main/weaker-shakedown transitions observed in the Cu(II) edges is reversed for Cu(III) (Figure 4). The latter observation is illustrated most dramatically in second derivative spectra. Parallel trends have been noted in the main and satellite peaks in 2p X-ray photoelectron studies of $Cu^{II}O$ and the Cu(III) oxides.[50,52,54]

For Cu(II) complexes, the lower energy shakedown peak has been associated with a primarily $|3d^{10}\underline{L}\rangle$ final state (i.e., formally a $2e^-$ transition, with LMCT accompanying the 1s → 4p transition), while the main peak is primarily due to transitions into the pure $|3d^9\rangle$ final state (Figures 1 and 5).[39] For Cu(III), the shakedown peak corresponds to a $|3d^9\underline{L}\rangle$ final state, and the main peak to $|3d^8\rangle$. The trend toward more intensity in the shakedown peak in Cu(III) complexes reflects a greater contribution of the charge-transfer configuration in the final state, as expected for a metal in a higher oxidation state. In the presence of a photoexcited 1s hole on the copper, the remaining electrons on the metal relax. Higher charge on the metal brings about deeper relaxation of its electrons, drawing more electron density from the ligand onto the metal in the excited state. Hence, the $2e^-$ transition gains in intensity for more highly charged Cu(III), relative to Cu(II).

An approximate analysis of the 1s → 4p transitions (main and shakedown) in edges for $[Cu^{III}_2(\mu\text{-}O)_2(L_{ME})_2]^{2+}$ and $[Cu^{II}_2(\mu\text{-}OH)_2(L_{ME})_2]^{2+}$, using the configurational interaction (CI) model developed by Sawatsky and co-workers,[55−57] supports these chemical expectations. Sets of ground-state parameters (Δ, *T*) for Cu(II) and Cu(III) were derived from previously reported analyses of XPS and XAS measurements on $Cu^{II}O$/$Cu^{II}Cl_4{}^{2-}$ and $NaCu^{III}O_2/La_2Li_{0.5}Cu^{III}_{0.5}O_4$.[39,52,59] These parameters, along with the measured energy separation between the two peaks (*W*), were used to calculate the remaining four parameters of the model. The model correctly predicts the observed oxidation-state-dependent trends in $I_{1s\rightarrow 4p}/I_{1s\rightarrow 4p+shakedown}$ and Cu/O covalency, using the given parameters (Table 3).

CI analysis predicts a median ~75% d-character in $[Cu^{II}_2(\mu\text{-}OH)_2(L_{ME})_2]^{2+}$, and ~57% in $[Cu^{III}_2(\mu\text{-}O)_2(L_{ME})_2]^{2+}$. The calculated d-character in the latter case may be a lower bound. The CI model used treats all ligands to the metal as equivalent; however, while this may be reasonable for OH^- and other ligands on Cu(II), the covalent bonding of O^{2-} will be far greater than that of amine. Parameters used in the analysis were derived from XPS studies on Cu(II)/Cu(III) with four equivalent oxide ligands. In addition, the molecular orbitals giving rise to the LMCT (i.e., shakedown) accompanying the 1s → 4p transition must be oxygen based. Covalency estimates from the model will therefore not quantitatively account for the amine ligands. The 2 eV increase in energy observed for the preedge for $[Cu^{III}_2(\mu\text{-}O)_2(L_{ME})_2]^{2+}$, relative to $[Cu^{II}_2(\mu\text{-}OH)_2(L_{ME})_2]^{2+}$, supports the conclusion that the predicted covalency for this molecule is likely an overestimate. The expected trend of increased covalency in the $Cu^{III}-O^{2-}$ bond, relative to $Cu^{II}-OH^-$, however, is correctly predicted from the data.

Mixed-Valence Species: Analytical Potential of K-edges. Cu K-edge XAS has previously been used to quantitate the amounts of Cu(I) and Cu(II) in mixed valence systems, with good sensitivity.[74] The intense 1s → 4p feature at ~8984 eV for Cu(I) allows it to be distinguished from Cu(II), which typically does not absorb strongly at this energy. In addition, the Cu(II) K-edge also has a low-intensity 1s → 3d preedge transition, which d^{10} Cu(I) lacks. To examine the analytical value of using the Cu K-edge to characterize mixtures of Cu(II) and Cu(III), the K-edge of a localized mixed-valence ($Cu^{II}Cu^{II}Cu^{III}$) trinuclear copper cluster[30] was measured (Figure 7). The mixed-valence cluster has the benefit of allowing for characterization

(72) Guo, J.; Ellis, D. E.; Goodman, G. L.; Alp, E. E.; Soderholm, L.; Shenoy, G. K. *Phys. Rev. B* **1990**, *41*, 82−95.

(73) Wong, J.; Lytle, F. W.; Messmer, R. P.; Maylotte, D. H. *Phys. Rev. B* **1984**, *30*, 5596−5610.

(74) Nguyen, H.-H. T.; Nakagawa, K. H.; Hedman, B.; Hodgson, K. O.; Chan, S. I. *J. Am. Chem. Soc.* **1996**, *118*, 12766−12776.

of Cu(III) alongside an internal Cu(II) comparison. The edge features that most clearly distinguish Cu(II) and Cu(III) are the preedge- and overall edge-energy shifts. Also, the energy splitting and intensity distribution of 1s → 4p + shakedown and the higher-energy 1s → 4p transitions and shifts in multiple scattering (MS) resonance energies reflect the presence of Cu(III). However, the 1s → 4p and 1s → 4p + shakedown transitions may be difficult to distinguish from the background rising edge absorption. The MS shifts are likely due to the contraction of Cu−ligand bond lengths, and therefore only indirectly reflect oxidation state.[49] Edge and preedge energy shifts were therefore considered the most likely candidate indicators of the presence of Cu(III) in the cluster.

The site-symmetries of the three coppers in the cluster are similar: square-planar N_2O_2 coordination, with each copper having two oxide and one bidentate diamine ligand. One of the three coppers differs from the other two only in its short, crystallographically determined Cu−ligand bond distances (Cu^{III}−O ∼1.84 Å, Cu^{III}−N 1.95 Å; Cu^{II}−O ∼1.98 Å, Cu^{II}−N ∼2.00 Å).[30] On this basis, and consistent with calculations, the molecule was described as a (class II) localized mixed-valent $Cu^{II}Cu^{II}Cu^{III}$ cluster.[75] Since the cluster is composed of two coppers, each with a local geometry similar to one of the coppers in $[Cu^{II}_2(\mu\text{-}OH)_2(L_{ME})_2]^{2+}$, and one copper with a local geometry like either copper in $[Cu^{III}_2(\mu\text{-}O)_2(L_{ME})_2]^{2+}$, edge data for the cluster should be approximately simulated by adding data for these two complexes, in a 2:1 ratio. The edge for the trinuclear cluster is indeed remarkably well simulated by such an addition (Figure 7B).

Comparing the edge for the trinuclear cluster to edges for $[Cu^{II}_2(\mu\text{-}OH)_2(L_{ME})_2]^{2+}$ and $[Cu^{III}_2(\mu\text{-}O)_2(L_{ME})_2]^{2+}$ (Figure 7A) shows that this edge is only slightly shifted toward higher energy, with respect to the $[Cu^{II}_2(\mu\text{-}OH)_2(L_{ME})_2]^{2+}$ edge. The trinuclear preedge is a plateau stretching across the 8979−8981 eV region, with no sharp peak at either the characteristic Cu(II) or Cu(III) energy, but with absorption over both regions. Thus Cu(III) is detectable via edge and preedge indicators, though subtly. The ls → 4p + shakedown transition is broad, and in the second derivative of the spectrum two peaks are detectable (Figure 7C). These peaks are of the same energies as the transitions observed in spectra for $[Cu^{II}_2(\mu\text{-}OH)_2(L_{ME})_2]^{2+}$ and $[Cu^{III}_2(\mu\text{-}O)_2(L_{ME})_2]^{2+}$, respectively, and are presumably due to 1s → 4p + shakedown transitions in the constituent Cu(II) and Cu(III) sites of the trinuclear cluster.

Even in this relatively simple, well-defined Cu(II)/Cu(III) mixed-valent material, the $^1/_3$ Cu(III) contribution to the edge is fairly subtle. Cu K-edges have been applied in a few cases to far more complex, mixed-valence materials, to determine whether a small amount of Cu(III) was present and in what fraction of the copper.[22,23] The current data suggest that Cu K-edges, while very useful for assigning oxidation state in mostly oxidation-state-pure materials, likely cannot be used to detect a small amount of Cu(III) in mixed-valence materials.

A Model Cu(II)-Phenoxyl. That the pure $|3d^8\rangle$ ground state for copper is energetically unfavorable is well documented. The repulsive electrostatic energy of the two d-orbital electron-holes (the Hubbard *U*) is greater than the charge-transfer energy (Δ) separating the ligand p from the metal 3d orbitals; hence the Cu(III) ground state is occasionally described simply as $|3d^9\underline{L}\rangle$, where $\underline{L}$ denotes an electron hole located on the coordinating ligand. However, this description alone is misleading. As the preceding analysis of main/shakedown transitions in the $[Cu^{III}_2(\mu\text{-}O)_2(L_{ME})_2]^{2+}$ edge suggests, the ground state is more appropriately described as a strongly covalently mixed contribution of $|3d^9\underline{L}\rangle$ and $|3d^8\rangle$ configurations.

An alternative type of $|3d^9\underline{L}\rangle$ system is available for comparison: a Cu(II) molecule that oxidizes to form a ligand radical (designated $\underline{L}$) directly coordinated to Cu(II). A few well-described examples of such molecules are known.[11−14,16] Many oxidize to form diamagnetic species, as the unpaired electron on the copper antiferromagnetically couples to the unpaired electron on the ligand. A more precise spectroscopic picture of the orbital nature of Cu^{II}-$\underline{L}$ has not been formulated. Existing examples of molecules of this type are oxidized at an anionic oxygen which itself is joined to an aromatic ring. Partial delocalization to the adjacent π-system is thought to stabilize the electron hole. The K-edge for one such compound, $[Cu^{II}\text{-}\underline{O}\text{-BDB}]^+$, is presented, along with the K-edge for its non-oxidized, Cu(II) counterpart, $[Cu^{II}BDB]$ (Figure 8).

These edges are considered with respect to features characteristic of Cu(III): the raised-energy preedge (∼8981 ± 0.5 eV), and a less well-defined general shift of the entire edge to higher energy, relative to the same-ligand Cu(II) compound. By either of these measures, the copper in Cu-$\underline{O}$-BDB is clearly Cu(II). The preedge for this compound appears at ∼8978.5 eV, at the lower end of the Cu(II) energy range. This may be a reflection of the presence of an especially weak-field ligand, the coordinated radical. Weak ligand field splitting would have the effect of lowering the energy of the recipient orbital of the 1s → 3d transition ($3d_{x^2-y^2}$), lowering the overall transition energy. The remaining features of the $[Cu^{II}\text{-}\underline{O}\text{-BDB}]^+$ edge appear at similar or slightly lower energies than corresponding features in the $[Cu^{II}BDB]$ edge. The edge for $[Cu^{II}\text{-}\underline{O}\text{-BDB}]^+$ is consistent with the EXAFS structure, where it is shown that the Cu−ligand bond lengths are not contracted relative to those in $[Cu^{II}BDB]$.[66] Thus there is no indication in the $[Cu^{II}\text{-}\underline{O}\text{-BDB}]^+$ edge that the charge on the copper is different from that in $[Cu^{II}BDB]$.

This is in contrast to what was observed for the Cu(III) compounds. In $[Cu^{II}\text{-}\underline{O}\text{-BDB}]^+$, the extra electron hole is stabilized through delocalization to the adjacent phenyl group. In $Cu^{III}-O^{2-}$, the hole is covalently shared between the oxygen and the copper. Edge and preedge energy shifts for the series of formally Cu(III) molecules in Figure 1 demonstrate the involvement of copper-centered orbitals in the stabilization of the electron hole, as the effective nuclear charge of the copper is increased.

Summary

Cu K-edge XAS provides a clear means of identifying Cu(III). A distinct feature of Cu(III) is a 1s → 3d transition centered on 8981 eV, ∼2 eV higher than the characteristic energy of this transition for Cu(II) complexes. This feature can be used to characterize Cu(III) analytically without having to refer to one or more Cu(II) K-edges for comparison. Cu(III) is identifiable when present at 1 part in 3 of a well-defined Cu(II)/Cu(III) mixture, though likely would not be detectable in proportions much lower than this. Analysis of the 1s → 4p transitions in a molecular $[Cu^{III}_2(\mu\text{-}O)_2L_2]^{2+}$ species shows a ground state where the two electron holes of the formally d^8 copper are covalently delocalized on the copper and oxide ligands. This is in contrast to the Cu(II)-phenoxyl system studied, which also has two electron holes, but in which there is no evidence of increased effective nuclear charge on the copper.

Acknowledgment. The authors gratefully acknowledge Dr. Yadong Wang (Department of Chemical Engineering, M.I.T.),

(75) Root, D. E.; Henson, M. J.; Machonkin, T.; Mukherjee, P.; Stack, T. D. P.; Solomon, E. I. *J. Am. Chem. Soc.* **1998**, *120*, 4982−4990.

Dr. Marc Schrier and Prof. Angelica Stacy (Department of Chemistry, University of California at Berkeley), Dr. Andrea Collier and Prof. J. M. Mayer (Department of Chemistry, University of Washington), and Dr. K. Fujisawa (Tokyo Institute of Technology) for providing samples for X-ray absorption measurements. J.L.D. acknowledges Dr. Thorsten Glaser (Department of Chemistry, Stanford University) for helpful discussions. This work was supported by NIH GM-50730 (T.D.P.S.); NIH RR-01209 and NSF CHE-9423181 (K.O.H.); and NIH DK-31450 (E.I.S.). SSRL is funded by the Department of Energy, Basic Energy Sciences, and the SSRL Structural Molecular Biology Program is supported by the National Institutes of Health, National Center for Research Resources, Biomedical Technology Program, and by the Department of Energy, Office of Biological and Environmental Research.

Supporting Information Available: Edge spectrum for $Cu^{II}(OC_6H_4$-*p*-F)(HB(3,5-$^{i}Pr_2pz)_3$). This material is available free of charge via the Internet at http://www.pubs.acs.org.

JA993134P